

## Multi phase-field simulation study on microstructural grain development during inductive-based friction surfacing of aluminium

D. K. Sahoo<sup>a,\*</sup>, B. S. Mohanty<sup>b</sup>, G. B. Bhaskar<sup>c</sup>

<sup>a</sup>*Asst. Professor, School of Mechanical Engineering, Sathyabama Institute of Science & Technology, Chennai, TN, India*

<sup>b</sup>*Professor, School of Mechanical engineering, Sathyabama Institute of Science & Technology, Chennai, TN, India*

<sup>c</sup>*Associate Professor, Dept. of Production Technology, MIT Campus, Anna University, Chennai, TN, India*

The computational solution is considered an effective tool for the analysis and a good understanding of the complex microstructural development that occurs during friction surfacing. In this article, ABACUS software was used to create a 3D-FE model of friction surfaced layering of AA 6063 aluminium on EN8 carbon steel, and the heat and strain rate collected throughout the operation were utilised for a computational investigation of microstructural recrystallization and grain development. The Multi-phase Field model (MFM) and constructive material model (CMM) were used for the prediction of the grain development during the process. A decrease in the incubation period from 0.839 sec to 0.578 sec was seen before recrystallization, after a temperature rises from 100°C to 300°C for substrate preheating. Validation of the reliability model obtained from the computational study was done using the image received from electron backscattered diffraction (EBSD) for grain size development and distribution. An appropriate assessment has been made between computational and experimental images which shows the maximum error of less than 10%. The development of grain structure during recrystallization was impacted extensively for increasing the coating strength, which was seen as inversely proportional to the average coating's grain diameter.

(Received December 8, 2021; Accepted February 23, 2022)

*Keywords:* Friction surfacing, Multiphase field model, Frictional recrystallization, Grain size

### 1. Introduction

Friction surfacing (FS) was invented by Nicholas during his patent work of joining dissimilar materials [1]. FS is a promising method of solid-state bonding for both similar or dissimilar materials. It produces an exceptional coating over the substrate where the fusion-based coating is extremely difficult. FS uses a mechtrode (coating material) in the form of a circular rod carrying downward axial force rotating at constant rotational speed over the substrate (base material). This causes frictional heat to build at the substrate coating contact, loosening the coating substance and the formation of a viscoplastic film there at the rod's tip, as well as the commencement of the diffusion mechanism. After a certain dwell period, the mechtrode was moved over the substrate, resulting in the deposit of plasticized coating material over the substrate and forming a metallic coating. The coating shape and mechanical characteristics are heavily influenced by the fundamental process parameters of FS, such as axial force, rotating speed, and transverse speed of the mechtrode. Changes in coating geometry and the mechanical strength were seen following an alteration in the process parameters. Generally, friction surfacing is a solid-state deposition process. Its process significance, heat generation, and the nature of plastic deformation (PD) help its effectiveness for the enhancement of the surface characteristics of the base materials through the interchange of its microstructure and chemical compositions [2,3]. After completion of

---

\* Corresponding author: dillipkumarsahoo@gmail.com  
<https://doi.org/10.15251/DJNB.2022.171.263>

the coating, the surface cooling was initiated by the transfer of heat towards the environment and the depth of the substrate. This cooling process helped the creation of fine-grain molecular structure and homogeneous coating. There is a likelihood of the occurrence of the distribution of second phase particles as a result of the thermal effect induced by friction surfacing and other developments that include phase transformation arising due to the chemical composition seen in the mechtrode materials.

As mentioned, the nature of the deposition in the FS process depends on the treatment received by the mechtrode during the viscoplastic stage which further implicit the behaviour of dynamic recrystallization during the process. The cooling process was started after the completion of the deposition process. Heat transfer occurred towards the environment and to the depth of the substrate. Effective cooling after deposition enabled a homogeneous bonding with fine-grained microstructural features due to the chemical compositions of the mechtrode. In plastic deformation (PD) involved industrial processes, Correlations between processing variables and the produced substructure are critical for production and system improvement. The influence of the development of grain refinement and grain structure at the coating on most of the structural and mechanical characteristics is seen in friction surfacing. Most of the properties like bond strength, hardness, toughness, plasticity, corrosion resistance witness effective enhancement at the reduced grain structure. Despite much experimental research work carried out for the analysis of the microstructural feature like grain development, grain size during friction surfacing of various material combinations. The influence of process parameters on microstructural development through the experimental study is quite expensive and also restricted to experimental trials. Hence, the prediction of microstructural features during friction surfacing through mathematical simulations is an effective method for gaining a clear and good perceptive knowledge about microstructural growth.

To date, many researchers have used different microstructure modeling techniques in carrying out numerical modeling of dynamic recrystallization and microstructure development throughout the frictional surfacing procedure. Grujicic et al [4] applied the FEM method for computation of temperature and strain rate during FSW and used certain values as inputs parameters for the Monte Carlo Model in the examination of the correlation between the formation of grain structure and grain refinement during DRX at different locations of the weld joint. Their studies have indicated the impact of temperature on the evolution of grain structure inside a heat-affected zone (HAZ), at the thermomechanically affected zone (TMAZ), and stirred zone. The Monte Carlo method uses a straightforward algorithm for calculating the rate of nucleation with the ability to predict the nature of grain size relatively in a large area. But this model does not produce realistic results where high-temperature deformation is involved. It does not consider the kinematics of grain development due to model restrictions. [5,6] In the field of material science, the cellular automaton (CA) model is a popular technique for modeling and analysis of the dynamic recrystallization behaviour of the materials due to its model advantage. Hallberg et al. [7] has simulated the grain structure during high thermal deformation of copper using the probabilistic CA model. A similar CA concept was utilized for the development of a three-dimensional presentation in the investigation of the influence of impurities during the dynamic recrystallization of copper [8]. Ding and Guo [9] used the coupled recrystallization kinetics and CA model for the formulation of the grain growth and nucleation rate of commercially pure copper during high-temperature deformation. The multi-scale computational model included the material's microstructural behaviour, the kinetics of grain boundary, and dislocation density. The same CA simulation model was used in the formulation of recrystallization behaviour during the processing of the  $\beta$  phase of Ti-6Al-4V alloy [10]. Popova et al. [11] have simulated the developed microstructural form and height of the recrystallized grains of magnesium alloys using the probabilistic CA technique. A similar type of analytical method was used in the simulation and assessment of dynamic crystallization characteristics of different materials like titanium alloys [12, 13], steel [14], and nitrogen alloy [15]. The Kocks-Mecking or KM model [16] was used in the simulation of the dislocation density and forecasting of grain size and grain structure kinetics during the plastic deformation stage. Buffa et al. [17] used two models for finding out the average grain dimensions in the continual dynamics recrystallization stage throughout friction stir welding (FSW) of AA7075 alloys. A quadratic error technique was also used for comparison of the results

of both the analytical methods and a good approximation related to the grain structure growth at the stir zone was found. Song et al. [18] simulated microstructural behaviour in the recrystallization stage during FSW welding of TA15 titanium alloy via the CA method. Their simulation work included a study of the behaviour of plastic deformation on a macro-scale through multi-scale modeling, the interaction of dislocation density on mesoscale, grain development, and the mechanical features of obtained FSW joints. Akbari et al. [19] combined the KM and Laasraoui-Jonas model for the modelling of microstructural development all through the FSW joining of AZ91 magnesium alloy. Using the KM model, they analysed the dislocation density based on the development of the strain rate. LJ models were used for microstructure analysis. Shojaeefard et al. [20] worked on the grain structure and microstructural growth during FSW joining of AA1100 aluminium alloy using both the modified LJ and CA models. They developed a good correlation between rotational speed, tool shoulder diameter, and transverse speed with grain size applying Taguchi's optimization technique. Saluja et al. [21] investigated the development of grain structure at the stir region during the FSW joining such as both like and different aluminium alloys using the CA model coupled with a finite element (CAFÉ) model. They saw good accuracy in the predicted grain structure and yield strength through the use of the simulation model and the experimental data. Miles et al. [22] studied the grain structure at the recrystallized phase during the friction joining of 304L stainless steel using both the Eulerian Finite element model (E-FEM) and the analytical approach. They found a maximum error of around 39% between the estimated grain size and the experimental values. In their work of simulation, Valvi et al. [23] and Asadi et al. [24] took considered both joined LJ and cellular CA models for estimating the microstructural dimensions of the recrystallized grains throughout FSW welding of AZ91 magnesium alloys. They utilized the model for building out the dislocation density, rate of nucleation, and grain development at the stir zone. Yang et al. [25] analysed the recrystallization phase and grain development at the stir zone of FSW joining of AA6061 aluminium alloys using both the multiphase-field (MPFM) and the KM dislocation methods. Their focus was on the growth of grain size on the effect of welding speed and found a constant ratio of around 30% between recrystallization to processing time by intensifying the welding rate but in the same way, the duration of the recrystallization period was decreased.

The available resources have confirmed the performance of the recrystallized microstructural simulation in friction-based deposition processes like friction surfacing (FS), friction stir welding (FSW) in a limited manner where the recrystallized grain development occurred due to the severe High-temperature plastic deformation with a high strain ratio. The available literature sources, Too far, there has been no access to the prediction of microstructural modification in the coating done by friction surfacing technique. The unique features of the friction surfacing process and its applications in repairing worn coatings, enhancing surface properties, and in the field of additive manufacturing have provided unique importance to the calculation and forecasting of coating microstructure for estimating the mechanical properties.

In this simulation study, analysis of the dynamic recrystallization and grain structure development of aluminium AA6063 coated over EN8 carbon steel by friction surfacing process was done by multiphase-field (MPFM). An established material model was also used for finding the dislocation density. The temperature field of the mechtrode and substrate was simulated using the finite-difference modelling technique. A model of heat source for both mechtrode and substrate was established during the friction surfacing process. The required data like temperature and strain rate were acquired from 3D- FE model (using abacus software) of the friction surfacing process for modelling the recrystallized microstructure and grain development. The experimental test helped estimation of the nature of dynamic recrystallization and grain structures. The influence of FS process parameters on grain size development was also analysed.

## 2. Materials and experimental setup

During this study, an aluminium 6063 rod (Mg-0.55 Si-0.4 Cr-0.1 Mn-0.1Fe-0.35 Ti-0.1 Al- Balance) a consumable rod with a length of 18 mm was employed during FS. An EN8 medium carbon steel plate (C- 0.36Mn-0.06 Si -0.1 P -0.05 S -0.05 Ni -0.01 Fe- Balance Wt%) with a

measurement of 150 x 70 x 6 mm<sup>3</sup> was chosen as the substrate material due to its nonmagnetic behaviour and poor corrosion resistance. The deposition process was carried out using a commercial friction surfacing machine. Before FS, the oxide layer present on the substrate plate was eliminated by the milling machine and a surface with constant roughness was maintained. The aluminium 6063 rod received was fastened to the spindle and maintained at constant travel speed during the friction surfacing. These were seen as more stable than constant axial force-feeding for the consumable rod. The specimens were produced under different combinations of process parameters like axial force (4 and 6 kN), rotational speed (1500 and 3000 rpm), and constant travel speed (150 mm/min). An induction unit (2kW) helped supply the heat for preheating the substrate plate for the achievement of the temperatures of 100°C, 200°C, and 300°C. A temperature-controlled regulator was used for control and achievement of the required substrate temperature before friction surfacing. An infrared thermometer was used for observation of the temperature development both on the oncoming and receding sides during coating. With an increase in surface oxidation and temperature, the emissivity of aluminium and EN8 carbon steel was taken as 0.86 and 0.32 respectively for the infrared testing as per the literature survey.

The samples were prepared using a wire to separate the samples cutting machine to a dimension of 5x5 mm<sup>2</sup> for the analysis of microstructural features. Initially, the metallographic specimens obtained from mechtrode, coating samples were polished using 60 to 4000 grit sandpaper. Their surface had undergone an electrolyte polishing with an electrolytic composition of 750 mL of methanol + 50 mL of HClO<sub>4</sub> + 200 mL of water at 25°C. FE- SEM and EBSD instruments were used for microstructure and crystallographic analysis.

*Table 1. Chemical Composition of EN8 Medium carbon Steel.*

Material	C	Mn	P	S	Si	Ni	Fe
% of composition	0.36	0.60	0.05	0.05	0.10	0.01	Balance

*Table 2. Chemical Composition of AA 6063 Aluminium Alloy.*

Material	Mg	Si	Cr	Mn	Ti	Zn	Fe	Al
% of composition	0.55	0.4	0.1	0.1	0.1	0.1	0.35	Balance

*Table 3. Parameter matrix for experimental work.*

Experiment No	Axial Force (kN)	Rotational speed (rpm)	Substrate Temperature(°C)
E1	4	1500	100
E2	4	1500	200
E3	4	1500	300
E4	4	3000	100
E5	4	3000	200
E6	4	3000	300
E7	6	1500	100
E8	6	1500	200
E9	6	1500	300
E10	6	3000	100
E11	6	3000	200
E12	6	3000	300

### 3. Mathematical modeling

#### 3.1. Model of frictional heat generation at mechtrode

Analysis of the frictional behaviour of the mechtrode during friction surfacing requires the assumption of the production of pressure and heat at the interface region as uniform. Together with the derivation of frictional heat at the substrate mechtrode interface from the mathematical formulation followed. An elemental annulus with an inner radius  $r_p$  and width  $dr_p$  was defined at the frictional interface before that. This is displayed in figure 1.

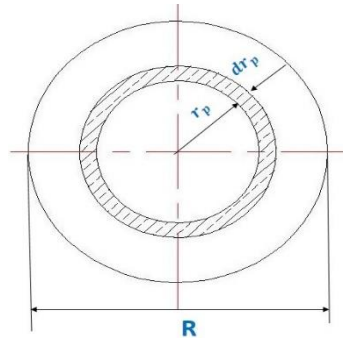


Fig. 1. Frictional interface of mechtrode rod.

A constant pressure ( $p_c$ ) was acting throughout the contact surface of the mechtrode. Therefore the area of the elemental annulus has been calculated as  $dA_p = (2\pi r_p) \cdot dr_p$  by converting the pressure equation into a differential representation of the area  $dA_p$ . The differential force  $dF_r$  which acting on the area  $dA_p$  can be rewritten using the following equation.

$$dF_r = p_c dA_p = 2p_c \pi r_p dr_p \quad (1)$$

Let  $dF_d$  be the differential frictional force which is equivalent and opposite of the normal force acting on  $dA_p$ . The  $dF_d$  can be written as

$$dF_d = \mu dF_r = 2\mu p_c \pi r_p dr_p \quad (2)$$

where  $\mu$  is considered as the coefficient of friction. It can be referred to as the tangential velocity,  $V_t$  which is the same at any point on the elemental section and can be expressed as

$$V_t = r_p \omega_a \quad (3)$$

where  $\omega_a$  is called the angular velocity and the differential power ( $dp_c$ ) developed during the rotation of mechtrode is defined as

$$dp_c = dF_d (V_t) \quad (4)$$

By putting the value of  $dF_d$  and  $V_t$  in equation (4) and integrating concerning  $r$ , the designation of frictional heating power ( $p_c$ ) developed at mechtrode interface can be derived as

$$P_c = \int_0^R 2\mu p_c \pi r_p^2 \omega_a dr_p = \frac{2}{3} \mu p_c \pi (R^3) \omega_a \quad (5)$$

The frictional heat flux ( $Q_{r_p}$ ) developed at the mechtrode interface can be calculated as

$$Q(r_p) = \frac{dp_c}{dA_p} = \mu p_c \omega_A r_p \quad (6)$$

There is an enhancement of the material's physicochemical qualities caused by a temperature fluctuation during the plastic deformation of materials. During deformation analysis, variation in the established relationship among material and induced thermal strain is seen based on the temperature distribution during the process of heat transfer stage. The material deformation influences the heat transfer space, energy transition, and boundary condition of the mechtrode.

The power required for plastic deformation or the rate of internal energy ( $q_h$ ) available for the ductile mechtrode like aluminium which is away from the contact interface and can be written as

$$q_h = \beta_{eq} \sigma_{eq} \varepsilon_{eq} \quad (7)$$

where  $\beta_{eq}$  is the thermal efficiency during plastic deformation,  $\sigma_{eq}$  is the correspondent stress, and  $\varepsilon_{eq}$  is the equal strain value respectively. Based on the plastic deformation theory, the maximum amount of plastic deformation is converted into heat. The thermal efficiency  $\beta_{eq}$  is usually set as 0.9 (Zhang et al. [26]). The energy remaining is stored as dislocation and vacancy. For the aid of simplicity, during this computational analysis, the internal energy value was neglected as its value was very low compared to the frictional heat developed during the process.

### 3.2. Model of frictional heat source at the substrate

In friction surfacing, the total process is seen as having two consecutive stages i.e. the initial frictional preheating stage and steady deposition stage. At the beginning of the friction surfacing, the heat generated by friction at the surface of the substrate developed is the prime source for recrystallization of mechtrode material. After the preheating stage, the mechtrode experiences a severe plastic deformation, and the frictional interface is transferred to the coating layer position.

The total substrate thickness during substrate simulation is taken as  $Mt + St$  by considering coating thickness ( $Mt$ ) and substrate thickness ( $St$ ). A transient flux of local heat transfer can be applied over the total substrate thickness. This is shown in figure 2. The thermal exchange between the substrate and the surrounding atmosphere is also taken into account for simulation and expressed in the following terms.

$$-\lambda \frac{\partial T}{\partial n} = \alpha(T - T_a) \quad (8)$$

where,  $\lambda$ ,  $T$  and  $T_a$  are the thermal conductivity, temperature attained by the substrate, and atmospheric temperature respectively.

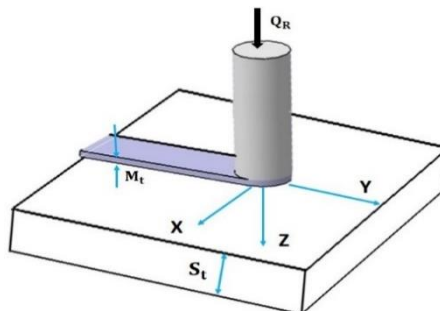


*Fig. 2. Heat source model of substrate.*

### 3.3. Thermo-mechanical model at coating interface

Development of temperature and strain rate at coating interface is the pre-requirement variable for carrying out the numerical simulation in the dynamic recrystallization period through the distortion of aluminium over medium carbon steel using frictional surfacing. The value of temperature and strain rate are calculated numerically with the help of a thermo-mechanical model. ABACUS software which has precise description ability to predict the temperature as well as the strain rate in extreme plastic deformation was used for developing the computational model for the friction surfacing process. Figure 3 depicts a visual representation of the friction surfacing model. For getting accurate temperature and strain rate during FS, the dimensional parameters in modelling have been taken as same as with experimental conditions testing variables are the same as the process parametric conditions, which include axial force, rotating speed, and transverse speed. During finite element solution, the finer mesh was used at the mechtrode and its travelling distance over substrate whereas coarser mesh was used in the remaining part of the substrate for saving the computation time. The mechtrode is divided into 4184 three-dimensional 4-node with linear coupled elements and the substrate plate is divided by 60736 elements.

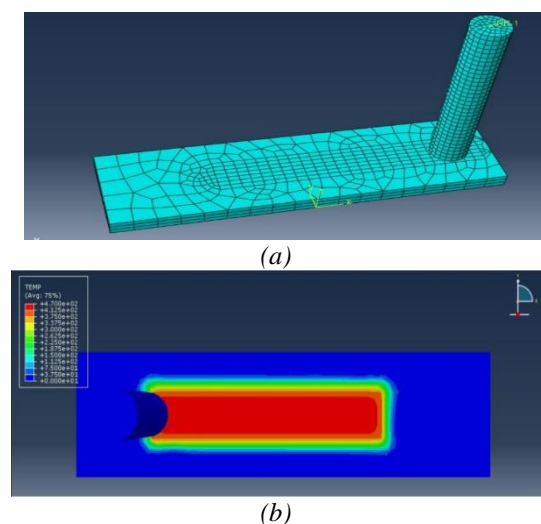


*Fig. 3. Schematic representation of friction surfacing model based on Abacus software during (a) meshing and (b) simulation.*

Material advancements during plastic deformation were considered as input and output flow for the employment of the axial force and mechtrode transverse speed on the top of the Eulerian surfaces as displayed in figure 4. Application of Coulomb's Law of Friction was done for consideration of the tangential movement of the interfacial surface concerning the contact condition of mechtrode. The ABAQUS/Explicit model simulation was used for solving all the developed equations for the thermomechanical model. The explicit mode of analysis required less time for model formulation in the friction surfacing process. This explains its preference for implicit model simulation. The complex dynamic problem requiring minimum time with précised solution can be resolved by applying ABAQUS/Explicit formulation [27]. The thermo-physical and elastic modulus properties used for friction surfacing modelling of both aluminium 6063 and EN8 carbon steel are displayed in Tables 4 & 5 respectively based on the available data in [28].

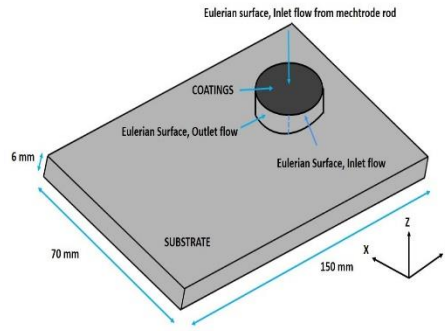


Fig. 4. Numerical domain of the friction surfacing process.

Table 4. Material characteristics of Aluminium 6063 alloy utilised in the analysis.

	Temperature range			
	@25°C	@100°C	@200°C	@300°C
Density (kg/m <sup>3</sup> )	2690	2656	2623	2602
Thermal Expansion (10 <sup>-5</sup> /°k)	2.34	2.42	2.56	2.68
Thermal Conductivity (W/m°C)	208.6	214.4	221.7	224.2
Heat capacity (J/g°C)	0.920	0.976	1.020	1.062
Young's Modulus (GPa)	68.9	68.3	67.4	65.2

Table 5. Material properties of EN8 carbon steel used in this analysis.

	Temperature range			
	@25°C	@100°C	@200°C	@300°C
Density (kg/m <sup>3</sup> )	7850	7842	7816	7783
Thermal Expansion (10 <sup>-5</sup> /°k)	0.59	0.61	0.65	0.69
Thermal Conductivity (W/m°C)	45.1	45.8	46.6	47.8
Heat capacity (J/g°C)	2.3	2.44	2.57	2.73
Young's Modulus (GPa)	192	191.4	190.3	189.1

The use of three-dimensional thermo-mechanical simulation in the FS process was made for the prediction of the development of temperature and distribution of strain rate. The effect of interface temperature significantly on the flow stress of the material requires the consideration of simultaneously both thermal and mechanical problems during the simulation. In this present analysis, the coupled thermo-mechanical simulation was used for finding out the thermal and mechanical behaviour of the materials during friction surfacing. For this analysis, substantial heat sources were developed as a result of the frictional contact and the material's plastic distortion which allowed alterations to thermo-mechanical characteristics in the material. Computation of the velocity field was done following the principle of conservation of momentum and by reducing the potential energy function (II) which is expressed as

$$\int \rho_d a_v v_v dV_e - \int F_V v_v dV_e - \int (\rho_d n_0) v_v dS_e - \int \sigma_t \varepsilon_r^* dV_e = 0 \quad (9)$$

where  $V_e$  and  $S_e$  symbolize the element of volume and surface respectively. Other parameters like  $a_v$ ,  $F_V$ ,  $v_v$ ,  $n_0$ ,  $\varepsilon_r^*$  and  $\sigma_t$  denotes the acceleration vector, volume force, virtual velocity field, outward normal, strain rate, and stress tensor respectively.

Using the mechanical model, the rate of heat generation was determined and expressed by the following terms

$$Q_g = \eta_p S_{Tij} \varepsilon_{rij}^{pl} \quad (10)$$

In Eq. (10),  $\eta_p$  is heat absorption caused by plastic deformation, the term  $S_{Tij}$  and  $\varepsilon_{rij}^{pl}$  are called the tensile stress and the plastic strain rate tensors respectively.

The following relationship was used for finding the heat formation at a substrate coating interface ( $q_{cr}$ ) during friction surfacing. [27]

$$q_{cr} = \mu_f P_c \gamma_s \quad (11)$$

where  $\mu_f, P_c, \gamma_s$  is the friction coefficient, pressure coefficient, and slip rate coefficient respectively

The use of a transient heat transfer equation proportionating it to the friction surfacing process is required for the assessment of the thermal response behaviour of the material. The transient heat transfer rate equation used for this study is expressed as:

$$\rho c_p \frac{\partial T_e}{\partial t} = \frac{\partial}{\partial x} \left[ (k_{th})_x \frac{\partial T_e}{\partial x} \right] + \frac{\partial}{\partial y} \left[ (k_{th})_y \frac{\partial T_e}{\partial y} \right] + \frac{\partial}{\partial z} \left[ (k_{th})_z \frac{\partial T_e}{\partial z} \right] + Q_g \quad (12)$$

where,  $c_p$  and  $k_{th}$  are the specific heat and the thermal conductivity of the material. (Symbol of x, y, and z refer to the thermal conductivity in three directions)  $Q_g$  is the rate of heat generation and  $T_e$  is the temperature calculated by the mechanical model.

The thermal efficiency at the substrate-mechtrode area of contact is taken into account as  $1000 \text{ W/m}^2 \text{ }^\circ\text{C}$ . On the assumption of more than 90% of the frictional heat at the interface should be transferred to the substrate material and 100 % of the mechtrode frictional work should be transferred to heat. The thermal efficiency of the upper portion of the mechtrode/tool holding interface of the FS machine and the base emerge of the substrate are presumed as  $1000 \text{ W/m}^2 \text{ }^\circ\text{C}$ . For the surrounding environment, the heat transfer coefficient was set at  $20 \text{ W/m}^2 \text{ }^\circ\text{C}$ . Using Johnson- Cook relationship, the mechanical characteristics and flow stress of the deposition metal expressed were related to various strain rates, and temperatures are stated:

$$\sigma_t \gamma_s = \left[ A_y + B_h (\varepsilon_{eq}^{-pl})^s \right] \left[ 1 + C_s \log (\varepsilon_{eq}^{-pl} / (\varepsilon_{eq})_R^{-pl}) \right] \left[ 1 - T_H^{ms} \right] \quad (13)$$

where,  $\varepsilon_{eq}^{-pl}, \dot{\varepsilon}_{eq}^{-pl}$  and  $(\varepsilon_{eq})_R^{-pl}$  are the equivalent plastic strain, equivalent plastic strain rate, and reference equivalent plastic strain rate respectively. Similarly,  $A_y, B_h, s, C_s$  and  $ms$  is known as the amount of the yield stress at the reference temperature, strain-hardening constant, strain-hardening exponent, constant strain rate, and thermal softening coefficient respectively. The homologous temperature developed during the friction surfacing is expressed by the following relationship.

$$T_H^{ms} = \left( \frac{T_o - T_r}{T_m - T_r} \right) \quad (14)$$

where,  $T_o, T_r$  and  $T_m$  are the current, reference, and melting temperature of the mechtrode in terms of Kelvin respectively. Relating to the data provided in [27], the values for the parameters used in the Johnson-Cook model are shown in Table 6.

Table 6. Parameters values of Aluminium 6063 alloy used in Johnson-cook strength model.

Representation	Units	Value
$A_y$	MPa	376
$B_h$	MPa	692
$s$	N/A	0.75
$C_s$	N/A	0.0085
$T_r$	K	298
$T_m$	K	793
$m$	N/A	1.72

### 3.4. Recrystallization model

A microscale (intra-granular) model combined with the mesoscale (inter-granular) model was used for the granular growth and recrystallization assessment during the friction surfacing of aluminium. The dislocation density within the grain structure in the microscale model was estimated using the Kocks-Mecking (KM) dislocation model while the MPFM mesoscale model was used for simulating the dynamic recrystallization and grain growth following the law of recrystallization. In the dynamic recrystallization simulation, the two-dimensional region was selected due to its low computational cost and good efficiency. A phase-field model coupled with a finite element model was used in the investigation of the grain size development. The flow chart showing the development of the recrystallization modelling is displayed in figure 5.

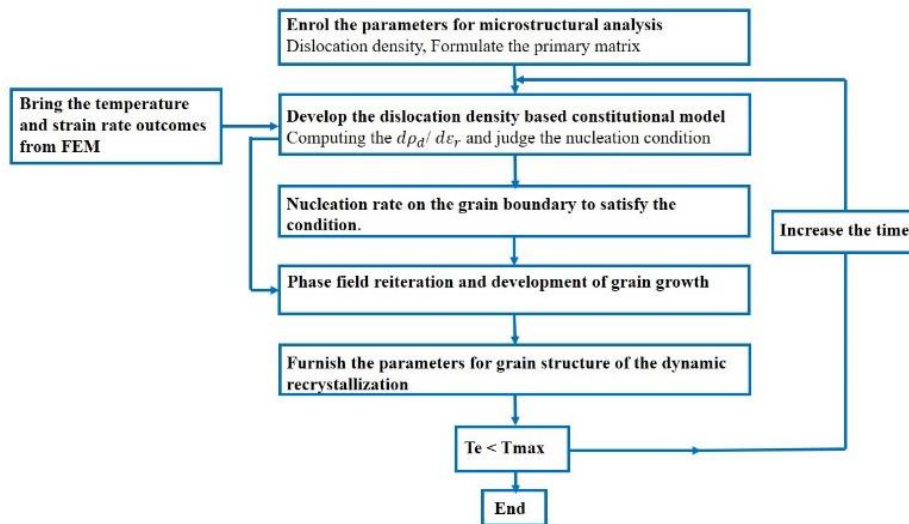


Fig. 5. Flow chart for recrystallization model during friction surfacing.

Using the Kocks-Mecking (KM) model [16, 28], the dislocations collections owing to plastic deformation was explained as the following expression

$$\frac{d\rho_d}{d\varepsilon_r} = Hc \left( \sqrt{\rho_d} - \frac{\rho_d \alpha_F \mu_s b v}{A_{f1} \varepsilon_r \exp\left(\frac{Q_{da}}{RT_e}\right)^{A_{f2}}} \right) \quad (15)$$

where  $d\rho_d$  and  $d\varepsilon_r$  denote the changes in dislocation density ( $\rho_d$ ) and strain ( $\varepsilon_r$ ) per unit time respectively.  $Hc$  is the hardening coefficient and  $\alpha_F$ ,  $A_{f1}$ ,  $A_{f2}$  are the fitting coefficients.  $Q_{da}$ ,  $R$ ,  $\mu_s$ ,  $b_v$ ,  $\varepsilon_r$  and  $T_e$  are the deformation activation energy, gas constant, shear modulus, burgers vector, strain rate, and temperature respectively. The temperature and strain rate were taken directly using the calculations of the FEA model and incorporated into the equation. A critical density of dislocations ( $\rho_{cc}$ ) was taken into account for identifying the onset for both dynamic recrystallization and grain development mechanism. According to Peczak and Luton models [29], the nucleation rate per unit area ( $N_r$ ) for grain boundary is a function of temperature and strain rate which is calculated by the following expressions.

$$N_r(\varepsilon_r T_e) = c_e \varepsilon_r^{m_e} \exp\left(-\frac{Q_{da}}{RT_e}\right) \quad (16)$$

where  $C_e$  and  $m_e$  are the parameters which experienced variations based on the experimental results. Each grain boundary has a lattice node, a new grain ( $\Phi N_u$ ) was developed where the nucleation requisites were established [25].

$$\Phi N_u = (N_r \Delta t n_{gb} dx dy / \delta t)^{-1} \quad (17)$$

where  $n_{gb}$  is the overall quantity of grain boundaries at each lattice position when the dislocation density value exceeds the critical nucleation rate and  $\delta t$  is known as the thickness of grain constraint. During phase-field modelling, a separate physical field was allocated for each grain, and the parameter  $\varphi_g$  (where represents the grain number) was taken as the presentation of each grain.  $\varphi_g$  was set as 1 and 0 for inside and outside of the grain and between 0 to 1 for the interfacial grains respectively. During the dynamic recrystallization process, the order parameters ( $n$ ) of developed grains were randomly chosen at a range from 1- 36 in such a way that the order parameters between the neighbouring grains should not be the same. According to Takaki et al. [30], the dynamic recrystallization model for a friction surfacing process can be expressed by the following equation.

$$\Phi_g = -\sum_{j=1}^n \frac{2M_{gj}^\phi}{n} \left[ \sum_{k=1}^n \left\{ (Z_{gk} - Z_{jk}) \Phi_k + \frac{1}{2} (e_{gk}^2 - e_{jk}^2) \nabla^2 \Phi_k \right\} - \frac{4}{\pi} \sqrt{\varphi_g \varphi_j} \mu b^2 (\rho_i - \rho_j) \right] \quad (18)$$

where  $M_{gj}^\phi$  is the phase-field mobility,  $Z_{gj}$  is the energy barrier height and  $e_{gj}$  is the coefficient of energy gradient respectively and they are mathematically presented in Eq.(19).  $\rho_i$  and  $\rho_j$  are known as the dislocation density of adjacent grains of  $g$  and  $j$ .

$$\left. \begin{aligned} a_{gj} &= \frac{2}{\pi} \sqrt{2\delta\gamma_{gj}} \\ Z_{ij} &= \frac{4\gamma_{gj}}{\delta} \\ M_{gj}^\phi &= \frac{\pi^2}{8\delta} M_{gj} \end{aligned} \right\} \quad (19)$$

where  $\gamma_{gj}$  and  $M_{gj}$  are the surface energy and the mobility of grain boundary respectively. Following the simplification of the equation, it can be assumed that all the grains have these mentioned boundary conditions like  $\gamma_{gj} = \gamma$ , and  $M_{gj} = M_g$ . The mobility of the grain boundary " $M_g$ " can be rewritten as

$$M_g = \frac{M_c}{T_e} \exp\left(\frac{-Q_{ae}}{RT_e}\right) \quad (20)$$

where  $M_c$  is a constant which can be taken from the experiment and  $Q_{ae}$  is the activation energy available during recrystallization. As per the data available in [25, 30-32], the detailed material parameters for MPFM and dislocation density models are summarized in table 7.

Table 7. Material parameters for MPFM and dislocation density-based constitutive model.

Symbol	units	value	Symbol	units	value
Hc	N/A	$4.4 \times 10^8$	$C_e$	N/A	$1.87 \times 10^{15}$
$\alpha_F$	N/A	0.54	$m_e$	N/A	1
$A_{f1}$	N/A	$2.1 \times 10^{44}$	$M_c$	$m^4 \cdot K \cdot J^{-1} \cdot s^{-1}$	0.746
$A_{f2}$	N/A	7.8	$Q_{ae}$	$KJ \cdot mol^{-1}$	95.2
$Q_{da}$	$KJ \cdot mol^{-1}$	148	$\delta$	$\mu m$	1
R	$J \cdot mol^{-1} \cdot K^{-1}$	8.314	$\gamma$	$J \cdot m^{-2}$	0.213
$\mu_s$	GPa	27.6	$\rho_{cc}$	$m^{-2}$	$5.48 \times 10^{13}$
$b_v$	A	2.53			

#### 4. Results and discussions

The use of the Finite component model for thermo-mechanical systems helped the achievement of the simulated value of temperature and strain rate. During friction surfacing, For all samples, a non-contact kind thermometer was employed to monitor the temperature at the substrate coating interface. Figure 6 shows a good understanding of the experimental and simulation results during the three steps of friction surfacing like heating, cooling, and maximum temperature. Figure 7 shows the results coming from both experimental measurements and simulation for all obtained samples. A temperature difference of  $36^\circ C$  (maximum) and  $17^\circ C$  (minimum) was seen in the sample obtained from E12 and E7 parametric conditions. After finding the temperature and strain rate at different locations of the coating, they were stated as a time function before being brought into the recrystallization model simulation as an input parameter.

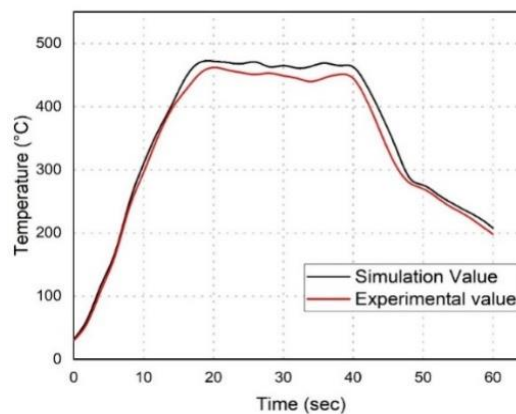


Fig. 6. Temperature comparison between the simulation and experimental values during friction surfacing at the substrate/coating contact.

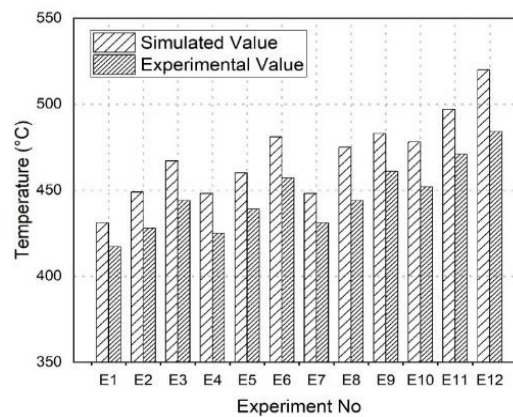


Fig. 7. Temperature variation between simulated and experimental values of samples from all parametric combinations.

Figure 8 depicts the evolution of temperature and strain rate for both cross-sections, and contact surface of the coating obtained from E7 parametric combinations in a steady-state condition. The absence of any major temperature difference between the advancing and retreating sides of the mechtrode is seen due to the high thermal conductivity of the mechtrode material. The increasing temperature and strain rate occurred at the advancing side of the coatings. The development of velocity vectors is mainly due to the rotational and transverse speed of the mechtrode and a large number of velocity vectors are found at the advancing side rather than on the retreating side of the coating. The good influence of the available substrate temperature on the maximum temperature formation was seen. An increase in the substrate temperature was followed by an increase in the maximum temperature of the coating, buta too high substrate temperature caused severe plastic deformation which affected the coating efficiency. The strain rate and temperature development at the advancing side, retreating side, and central region for all samples are displayed in table8. The rotational velocity vector ( $V_v$ ) at the mechtrode tip and coating interface calculated were as  $V_v = M_r \times \omega_r$  (where  $M_r$  &  $\omega_r$  are the radius and rotational speed of the mechtrode respectively). With an increase in the radius of the mechtrode, the velocity vectors could increase with the attainment of their maximum value. Hence, the maximum temperature and strain rate can be expected near the central zone of the rod. On the other side, there is a considerable amount of heat loss has been seen at the periphery of the contact face of the mechtrode. As a result, a temperature drop may occur at the periphery region of the rod. This temperature drop can help the enhancement of the flow stress of the deposition material and a reduction in plastic strain rate can be expected in that peripheral zone.

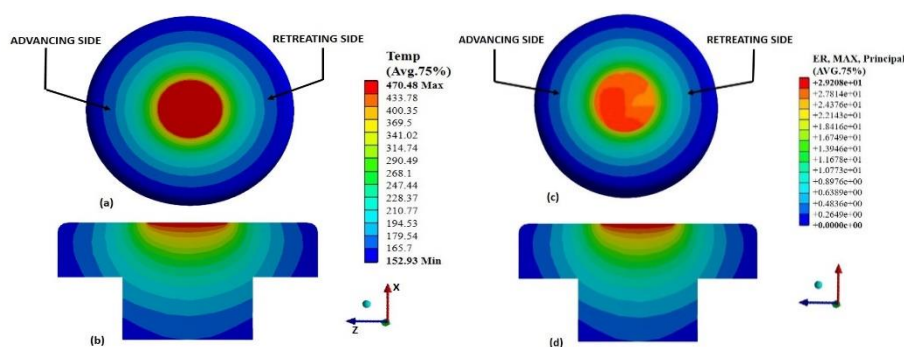


Fig. 8. The profile of mechtrode temperature at a) the top surface and, b) the cross-section and the strain rate profile at mechtrode top surface (c) and the cross-section (d) of the sample obtained at 100°C substrate temperature.

Table 8. Temperature obtained in a different region of coating for all parametric combinations.

Experiment No	The temperature at a different region of coating (°C)			Maximum Strain rate
	Advancing side	Retreating side	Central region	
E1	439±12	417±11	429±09	2.7818e+01
E2	457±14	433±08	448±11	2.8647e+01
E3	475±10	444±12	461±13	2.9412e+01
E4	456±09	422±08	438±14	2.9208e+01
E5	469±08	434±10	453±11	2.8716e+01
E6	490±10	467±13	481±10	2.9681e+01
E7	461±12	433±09	446±09	2.9414e+01
E8	483±10	448±12	464±12	3.0696e+01
E9	492±07	466±09	481±08	3.1278e+01
E10	486±09	452±13	474±11	3.1015e+01
E11	506±11	478±08	493±07	3.1926e+01
E12	528±06	492±11	510±11	3.2748e+01

For microstructural analysis, the cross-section of the aluminium mechtrode was prepared with small pieces with dimensions of 5 x 5 x 5 mm<sup>3</sup>, and A FE-SEM fitted with EBSD instrument was used in the study of the microstructure and crystallographic nature of the specimen. The microstructure of the received mechtrode (aluminium 6063) and the initial microstructure were used for the dynamic recrystallization model. These are shown in figure 9 (a) and (b) respectively. The initial average microstructural grain dimensions for both experimental measurements and numerical simulation were taken as 26.58±3.46 µm and 32.38±2.86 µm respectively. Based on the temperature and strain rate profile, the development of the microstructure was modelled at different times as shown in figure 10. The analysis includes the time before the initiation of plastic deformation to the end of plastic deformation in a streamlined manner. For specimen obtained from E1 combinations (axial force 4kN, rotational speed 1500 at 100°C substrate temperature), the time study taken along streamlines coating involved 3.5486 s (before the initiation of plastic deformation), 0.6953 s (the time taken for reaching maximum strain rate), 0.1439 s (equivalent time required for recrystallization initiation), 1.811s (equivalent time required for complete the recrystallization) and 0.4129 s (equivalent time required to complete the plastic deformation). It was seen before the plastic deformation of the mechtrode material and there is no substantial change seen in the dimension and structure of the grains (refer to figure 9). This was mainly due to the lack of dislocation density in initiating the recrystallization process. Development of the grain initiation of the mechtrode material was not developed due to the fast thermal cycling seen during the friction surfacing process. Accumulation of grain dislocation started at the initial stage of deformation but its density did not reach a maximum level. Hence no more microstructural change was seen during the formation of a new recrystallized grain structure.

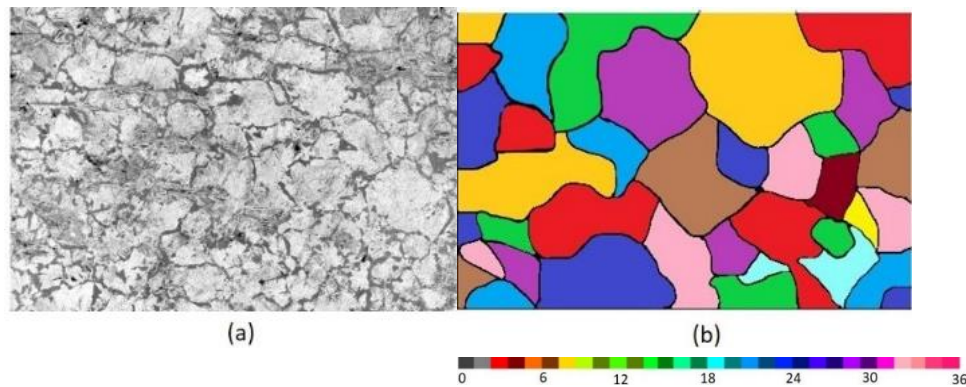


Fig. 9. The initial microstructure of the aluminium 6063 was obtained by a) optical microscopy and b) prediction by MPFM methods.

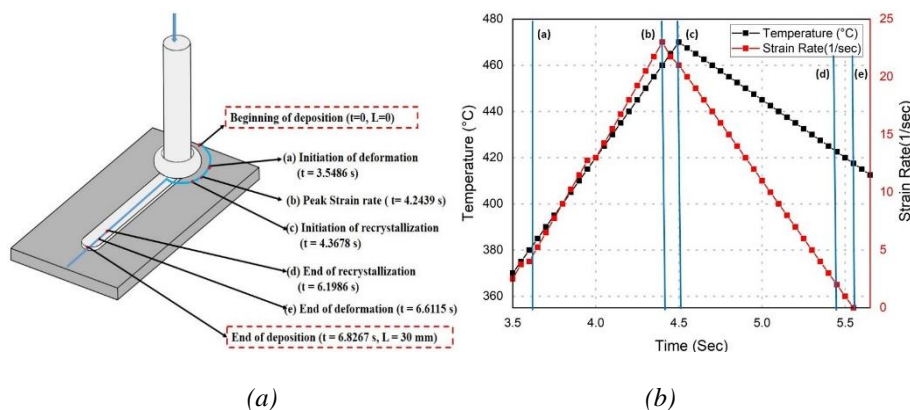


Fig. 10. Characteristic points (a) on the streamline by considering temperature and strain rate profiles (b) of the sample obtained at 100°C substrate temperature.

Deformation continued during the deformation stage and the strain rate was gradually increasing with a rise in the dislocation density. When the strain rate reached its maximum value of 0.6953 sec, the critical dislocation density was not completely found to initiate the recrystallization. After surpassing the maximum strain rate during the recrystallization period, the nucleation of new grains was started and the formation of new crystallized grain stopped at 1.811 sec due to the drastic decrease in the development of strain rate.

A comparative analysis has been made up between the experimental and predicted microstructures following the friction surfacing and simulation. This is displayed in figure 11. Taking into consideration of Eqns 15, 16, 17 & 18 at a constant temperature, the occurrence of the development of grain dislocation can be seen. Subsequently, the duration for the recrystallization period and the growth of recrystallization nuclei were also shortened. As a result, there was an increase in the formation of new grains during coating. With the variation of dislocation density between the raw mechtrode material and the crystallized grains being more, the growth of recrystallized grain structure was also more. The influence of the temperature available at the coating interface on the grain growth rate was seen. The borderline of nucleation experienced a reduction following an increase in the rate of grain growth during the process. But the duration of plastic deformation was rather short. Hence, in this simulation study, the influence of temperature and boundary variance and the nucleation rate during deformation was not taken into credit. The effect of temperature and strain rate on grain development during the recrystallization period of the FS process alone was observed. The subsequent results are displayed in figure 11.

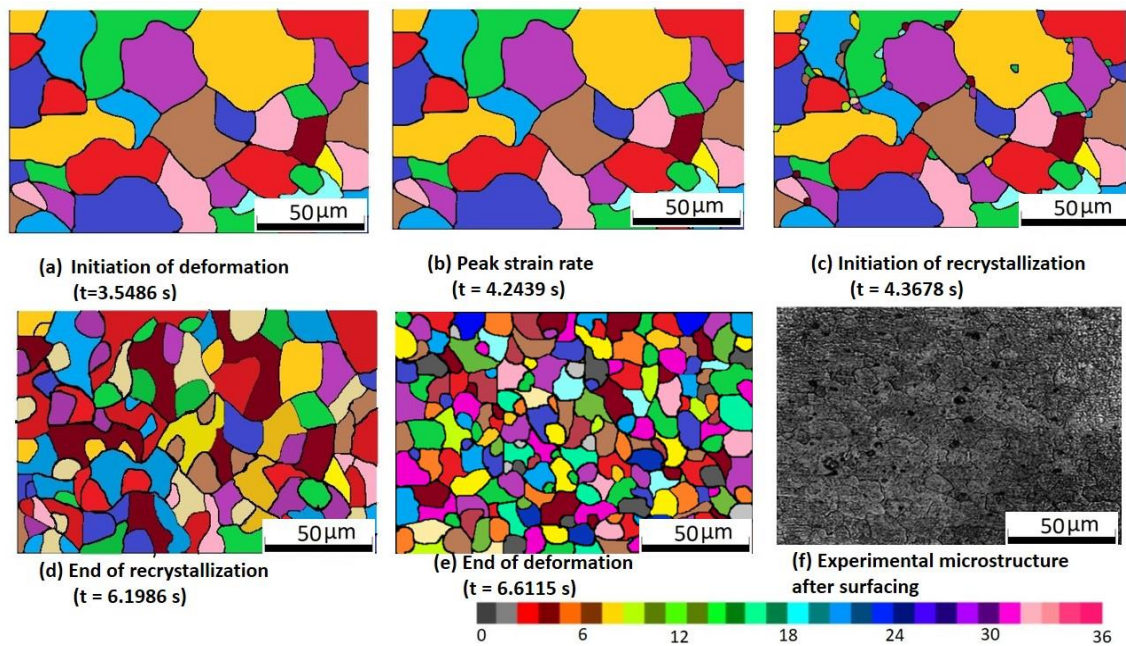


Fig. 11. Calculated microstructure at various feature points and experimental microstructure of sample at 100°C substrate temperature.

Figure 11 displays the computational grain development at the coating interface during friction surfacing with a parametric combination of the rotational speed of 1500 rpm, axial force 4 kN and substrate preheat temperature of 100°C. As shown in figure 11(a), when the plastic deformation initiates at time instant  $t = 3.5486$  s the accumulation of dislocating grains just started and no development of new crystals was seen as the dislocation density did not reach its critical value. Thus, a limited number of metal crystal grains were seen growing slowly during that process due to a temperature rise. With the progress of time, the strain rate started increasing (Figure 10). Accumulation of dislocating grains also started rising. Even after reaching the peak strain rate at  $t = 4.2439$  s, the dislocation density did not reach its critical value and so the recrystallization process did not start. After surpassing the peak strain rate at  $t = 4.3678$  s the recrystallization nucleation process started and then at the time  $t = 6.1986$  s the recrystallization nucleation process ends as the strain rate during the process decreased rapidly (Figure 10). The recrystallization nucleation was completed much before the completion of plastic deformation shown in figure 11 (d). The final grain development and distribution after completion of plastic deformation are shown in figure 11 (e).

The duration of various characteristic points for different substrate temperatures is shown in figure 12. The substrate preheating temperature is seen as having a great influence on the development of interface temperature and strain rate throughout the processing. A joint of axial force (4kN), rotational speed (1500 rpm), and 100°C substrate temperature, the interfacial temperature development, and strain rate are 440°C and 2.7818e+01 (refer to table 8) respectively which are low compared to other parametric combinations. The requirement of a high incubation time (duration from initiation of deformation to initiation of recrystallization) is for the recrystallization of mechtrode material could be seen. The smaller rate of recrystallization nucleation led to the creation of fewer recrystallized grains at the coating interface. With the low strain rate leading to a larger period of recrystallization, a growing opportunity was required for recrystallization of grains during the process or else it will stop the recrystallization in a very short time at higher temperatures.

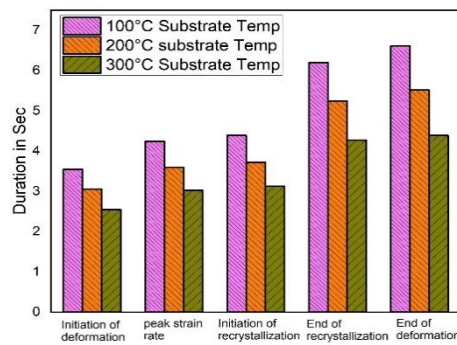


Fig. 12. Duration of various characteristics point of samples obtained from different substrate preheat temperatures. (4 kN, 1500 rpm).

Similarly, so when the substrate plate's pre-heating temperatures were elevated to 300°C, the temperature formation and strain rate are also increased with the requirement of a smaller incubation time for material recrystallization. As a result, a good recrystallization nucleation rate was developed and a larger number of recrystallized grains are formed at the coating interface.

A rise in the rotational speed caused a reduction in the duration of deformation and crystallization initiations which could be due to the formation of high substrate temperature at the coating interface.

Figure 13 shows the grain distribution attained by both experimental and simulated results of the mechtrode at different substrate preheats temperatures. Figure 13 (a) shows the grain distribution obtained at 100°C substrates preheat temperature. During plastic deformation, the strain rate was seen as low resulting in a slower accumulation of dislocation material and taking a long time for the nuclei to destroy the dislocation. The microstructural development was not continued till the end of plastic deformation. The low strain rate caused elongation of the duration of the recrystallization period with the grains having more opportunity to develop during the recrystallization process. When the substrate preheating temperature increased, the strain rate during plastic deformation also increased rapidly enhancing the accumulation of dislocating materials and taking a very short period to destroy the dislocation density of the material. This induced a high rate of recrystallization nucleation and less incubation period during the process, which further increased the development of new grains during coating. Figure 13 (b) and (c) show the grain development by experimental and numerical studies from the samples obtained by substrate preheating temperature 200°C and 300°C respectively. Based on the experimental and simulated results obtained from figure 13, a comparison has been made on grain characteristic values among the experimental and computational results which are listed in Table 9.

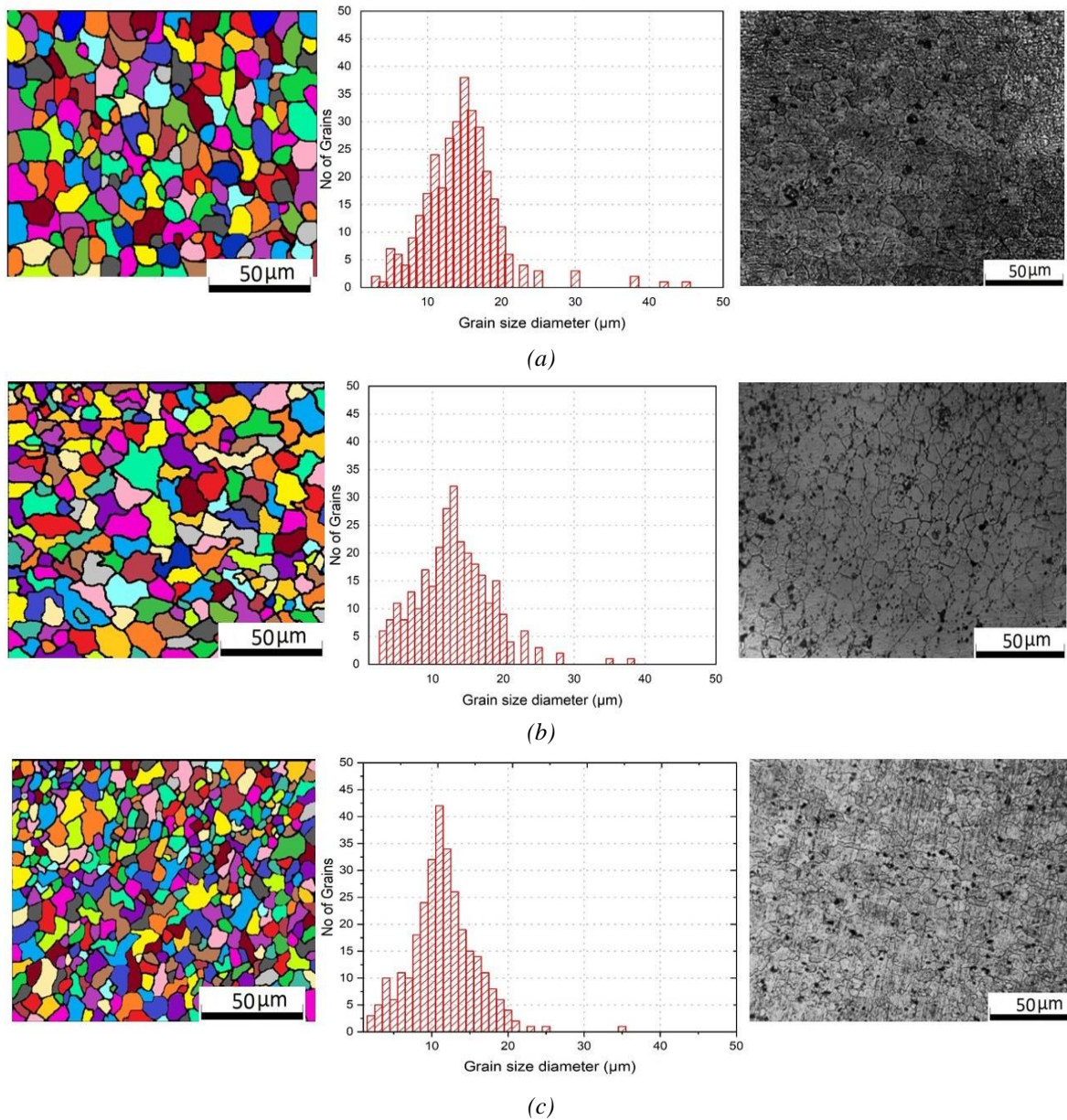


Fig. 13. Comparison of grain distribution at experimental and computational results of coating at different substrate preheating temperature (a) 100°C (b) 200°C (c) 300°C.

Table 9. Characteristics of grain shape values for experimental and computational results.

	Experimental Values			Computational values		
	Substrate Preheating temperature			Substrate preheating temperature		
	@100°C	@200°C	@300°C	@100°C	@200°C	@300°C
Average grain size (μm)	14.8	12.5	10.9	15.3	12.1	11.2
Size of most grains (μm)	14-16	11-13	9-10	16	11	10
The number of residual grains above 30 μm	15 or so	10 or so	6 or so	15	10	6

Table 9 shows a comparison of grain development of the samples from experimental and computational results at different substrate temperatures. The substrate preheat temperature was directly proportional to strain rate and interfacial temperature development during the process. The strain rate development at 100°C substrate preheats temperature was smaller than that of @200°C leading to a longer recrystallization period. Grain development during this period was adequate and the final size of the grains was distributed at a slightly higher range around 14.8  $\mu\text{m}$ . Overall, the average size of recrystallized grains was bigger as the number and shape of the mechtrode material were large. when the substrate preheats temperature increased to 300°C, the strain rate also increased and the rate of recrystallization nucleation was very high. As a result, the formation of large size residual mechtrode grains was reduced and at the same time, the duration of the recrystallization period was also shortened. The final size of the average grain structures is around 10.9  $\mu\text{m}$  and 11.2  $\mu\text{m}$  from experimental and simulation results respectively.

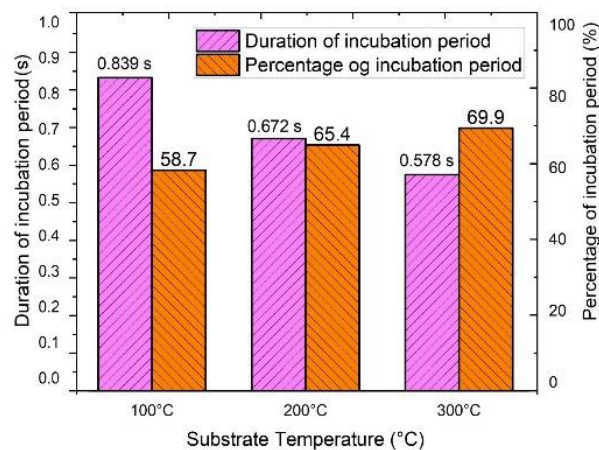


Fig. 14. Duration and percentage of incubation period with different substrate temperatures.

In the friction surfacing process, more attention has been given in this work to the recrystallization period for getting finer grains of the deposited material. Therefore, the acceleration of the recrystallization phase and the efficient utilization of the deformation stage for getting a continuous crystallization has been seen as the key factors. So a comparison has been made on the duration of the recrystallization incubation period and the available substrate preheating temperature. Figure 14, shows an increase in the substrate preheating temperature causing a shortening of the duration of incubation time. It is mainly due to the high rate of strain and faster dislocation of accumulating material. The friction surfacing process parameters influence the incubation period. With an increase in the rotational speed of the mechtrode, the duration of the deformation period decreased, and the recrystallization nucleation of material increased with a decrease in the incubation period.

Redefined arrangement of coating grain structure can provide better bonding strength, which is inversely proportional to a grain size that means the smaller size of the grain structure has a greater contribution to the bond strength [33]. The relation between the push-off strength and grain size of the coating is shown in figure 16. The conclusion is that the push-off strength of the coating can be increased by decreasing the grain size of the deposited materials. Overall the yield stress ( $\sigma_y$ ) is strongly depends on the grain size ( $l$ ) based on the Hall Petch relationship.

$$\sigma_y = \sigma_o + K_y.l^{0.5} \quad (21)$$

where  $\sigma_o$  and  $K_y$  represents the friction stress and positive yielding constant based on stress activity related to the adjacent unyielded grains.

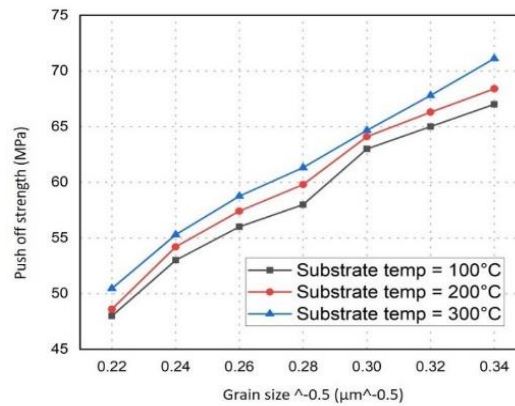


Fig. 15. Correlation between push-off strength and the square root of standard grain size.

#### 4. Conclusions

Numerical prediction of the grain development and recrystallization processes during the deposition of Aluminium AA6063 on EN8 carbon steel by friction surfacing was done utilizing a multiphase field model and dislocation density modelling. The achieved predicted model was validated by the experimental EBSD results to find the reliability. Based on the computational results under different process parameters, the following conclusions have been drawn.

1. Temperature and plastic strain rate increase adiabatically at the centre of the coating and then start decreasing towards the periphery of the coating. But the highest temperature and strain rate occurs at the advancing side and zone near to the central part of the coating respectively.

2. Low strain rate generates a smaller nucleation rate and retains a large number of parental metal grains which tends to increase the average grain size.

3. Application of the preheat temperature to the substrate causes an increase in the strain rate which leads to a reduction in the incubation and recrystallization period during friction surfacing. An increase in the preheating temperature from 100°C to 300°C, causes a decline in the incubation time before recrystallization from 0.839 sec to 0.578 sec.

4. The accumulation of dislocating materials is directly proportional to the rotational speed and formation of the plastic strain rate during friction surfacing. Higher rotational speed gives a higher rate of accumulating dislocation which needed more time for a dislocation to consume by nuclei. Hence, the recrystallization process continues till the end of the plastic deformation process.

5. Simulation results show that the finer size of the grains was achieved at high temperature and high strain rate conditions of friction surfacing. Finer grain size at the coating region enhances the push-off strength of the coating and by correlating between coating strength and the square root of the grain size, the Halle-Petch relationship was also established.

#### References

- [1] Klopstock, H, An improved method of joining or welding metals, Patent specification Ref.572789, 1941.
- [2] Pirhayati, P, Hamed JA, Surface and Coatings Technology 379 125059 (2019); <https://doi.org/10.1016/j.surfcoat.2019.125059>
- [3] Bararpour, SM, Hamed JA, Roohollah J, Journal of Alloys and Compounds 818 152823 (2020); <https://doi.org/10.1016/j.jallcom.2019.152823>
- [4] Grujicic, M, Ramaswami, S, Snipes, JS, Avuthu, V, Galgalikar, R, Zhang, Z. Journal of Materials Engineering and Performance, 24(9), 3471-3486; <https://doi.org/10.1007/s11665-015-1635-6>

- [5] Rollett, AD, Luton, MJ, Srolovitz, DJ, *Acta metallurgica et materialia*, 40(1), 43-55. (1992); [https://doi.org/10.1016/0956-7151\(92\)90198-N](https://doi.org/10.1016/0956-7151(92)90198-N)
- [6] Peczak, P, *Acta metallurgica et materialia*, 43(3), 1279-1291 (1995); [https://doi.org/10.1016/0956-7151\(94\)00280-U](https://doi.org/10.1016/0956-7151(94)00280-U)
- [7] Hallberg, H, Wallin, M, Ristinmaa, M, *Computational Materials Science*, 49(1), 25-34. (2010); <https://doi.org/10.1016/j.commatsci.2010.04.012>
- [8] Hallberg, H, Svendsen, B, Kayser, T, Ristinmaa, M, *Computational materials science*, 84, 327-338. (2014); <https://doi.org/10.1016/j.commatsci.2013.12.021>
- [9] Ding, R, Guo, ZX, *Acta materialia*, 49(16), 3163-3175 (2001); [https://doi.org/10.1016/S1359-6454\(01\)00233-6](https://doi.org/10.1016/S1359-6454(01)00233-6)
- [10] Ding, R, Guo, ZX, *Materials Science and Engineering: A*, 365(1-2), 172-179 (2004); <https://doi.org/10.1016/j.msea.2003.09.024>
- [11] Popova, E, Staraselski, Y, Brahma, A, Mishra, RK, Inal, K, *International Journal of Plasticity*, 66, 85-102 (2015); <https://doi.org/10.1016/j.iplas.2014.04.008>
- [12] Zhao, JW, Ding, H, Zhao, WJ, Cao, FR, Hou, HL, Li, Z Q, *Acta Metallurgica Sinica (English Letters)*, 21(4), 260-268 (2008); [https://doi.org/10.1016/S1006-7191\(08\)60047-2](https://doi.org/10.1016/S1006-7191(08)60047-2)
- [13] Chuan, W, He, Y, Wei, LH, *Computational materials science*, 79, 944-959 (2013); <https://doi.org/10.1016/j.commatsci.2013.08.004>
- [14] Chen, F, Cui, Z, Liu, J, Chen, W, Chen, S, *Materials Science and Engineering: A*, 527(21-22), 5539-5549 (2010); <https://doi.org/10.1016/j.msea.2010.05.021>
- [15] Zhang, Y, Jiang, S, Liang, Y, Hu, L, *Computational materials science*, 71, 124-134. (2013); <https://doi.org/10.1016/j.commatsci.2013.01.019>
- [16] Mecking, H, Kocks, UF, *Acta metallurgica*, 29(11), 1865-1875 (1981); [https://doi.org/10.1016/0001-6160\(81\)90112-7](https://doi.org/10.1016/0001-6160(81)90112-7)
- [17] Buffa, G, Fratini, L, Shivpuri, R, *Journal of materials processing technology*, 191(1-3), 356-359 (2007); <https://doi.org/10.1016/j.jmatprotec.2007.03.033>
- [18] Song, KJ, Dong, ZB, Fang, K, Zhan, XH, Wei, YH, *Materials Science and Technology*, 30(6), 700-711 (2014); <https://doi.org/10.1179/1743284713Y.0000000389>
- [19] Akbari, M, Asadi, P, Givi, MB, Zolghadr, P, *Modelling and Simulation in Materials Science and Engineering*, 24(3), 035012 (2016); <https://doi.org/10.1088/0965-0393/24/3/035012>
- [20] Shojaeefard, M. H, Akbari, M, Khalkhali, A, Asadi, P, Parivar, AH, *Materials & Design*, 64, 660-666 (2014); <https://doi.org/10.1016/j.matdes.2014.08.014>
- [21] Saluja, RS, Narayanan, RG, Das, S, *Computational materials science*, 58, 87-100 (2012); <https://doi.org/10.1016/j.commatsci.2012.01.036>
- [22] Miles, MP, Nelson, TW, Gunter, C, Liu, FC, Fourment, L, Mathis, T, *Journal of materials science & technology*, 35(4), 491-498 (2019); <https://doi.org/10.1016/j.jmst.2018.10.021>
- [23] Valvi, SR, Krishnan, A, Das, S, Narayanan, RG, *International Journal of Material Forming*, 9(1), 115-129 (2016); <https://doi.org/10.1007/s12289-015-1216-0>
- [24] Asadi, P, Givi, MKB, Akbari, M, *The International Journal of Advanced Manufacturing Technology*, 83(1-4), 301-311(2016); <https://doi.org/10.1007/s00170-015-7595-z>
- [25] Yang, C, Wu, C, Shi, L, *Science and Technology of Welding and Joining*, 25(4), 345-358 (2020); <https://doi.org/10.1080/13621718.2019.1706261>
- [26] Zhang, QZ, Zhang, LW, Liu, WW, Zhang, XG, Zhu, WH, Qu, S, *Science and Technology of Welding and Joining*, 11(6), 737-743 (2006); <https://doi.org/10.1179/174329306X153222>
- [27] Mandal, S, Rice, J, Elmustafa, AA, *Journal of materials processing technology*, 203(1-3), 411-419 (2008); <https://doi.org/10.1016/j.jmatprotec.2007.10.067>
- [28] Kocks, UF, *Laws for work-hardening and low-temperature creep* 76-85 (1976); <https://doi.org/10.1115/1.3443340>
- [29] Peczak, P, Luton, MJ, *Philosophical Magazine B*, 68(1), 115-144 (1993); <https://doi.org/10.1080/13642819308215285>

- [30] Takaki, T, Hisakuni, Y, Hirouchi, T, Yamanaka, A, Tomita, Y, Computational Materials Science, 45(4), 881-888 (2009); <https://doi.org/10.1016/j.commatsci.2008.12.009>
- [31] Sheppard, T, Wright, DS, Metals Technology, 6(1), 215-223 (1979); <https://doi.org/10.1179/030716979803276264>
- [32] Yao, Z, Kim, GY, Wang, Z, Faidley, L, Zou, Q, Mei, D, Chen, Z, International Journal of Plasticity, 39, 75-87 (2012); <https://doi.org/10.1016/j.ijplas.2012.06.003>
- [33] G. Dieter, Mechanical Metallurgy, third ed., McGraw-Hill, London, 1986.